A Grey-box Method for Stability and Controller Parameter Estimation in HVDC-connected Wind Farms based on Non-parametric Impedance

Mohammad Amin, *Member, IEEE*, and Marta Molinas, *Member, IEEE*

***Abstract*—Estimation of critical control parameters is a desirable tool feature for stability analysis and impedance shaping of high voltage dc (HVDC)-connected wind farms. Accurate estimation of such parameters would be enabled by access to detailed models, which is not always the case in real wind farms. Industrial secrecy is one of the main factors hindering the access to such models. This paper proposes a Grey-box method that, with basic assumptions about the control structure of the wind energy conversion system (WECS), can estimate the parameters of its controllers. The method is based on the measurements of frequency domain equivalent impedance combined with non-parametric impedance identification used in the solution of an inverse problem. The method makes possible to specify which part of the equivalent WECS impedance has a major impact on the stability of the system and according to this, re-shape the impedance to enforce stability. Once the critical controller bandwidth is identified with this method, an instability mitigation technique is proposed based on re-shaping the impedance by re-tuning the critical controllers of the interconnected converters. In order to avoid interaction between the HVDC rectifier and the WECS inverter, the controllers of both converters need to be re-tuned in such a way that the q-axis impedance magnitude of the HVDC system is kept lower than the q-axis impedance magnitude of the wind farm at the frequency of the phase-locked-loop bandwidth. The results show that the method ensures the stability of the system by re-tuning only the critical controller parameters.**

***Index Terms*—Non-parametric impedance Analysis, HVDC, Offshore wind farms, Stability Analysis, Impedance Analysis, Grey-box method.**

I. Introduction

THE impedance-based analysis, first presented in [1], has proven to be a useful tool to assess the stability of interconnected system of wind farms and high voltage dc (HVDC) transmission system [2]-[4]. The impedance measurement is the essence of the impedance-based approach for the Nyquist criterion to estimate the stability [5]. In order to apply this approach, deriving the analytical impedance model of the inverters is the prerequisite and the correctness of the analytical impedance model is verified by numerical simulations or experiments [6]-[13]. The analytical impedance model is a continuous transfer function and the Nyquist criterion is verified on the transfer function of the source-load impedance ratio. To derive the analytical model of the impedances, a detailed modeling of the power electronics converter's control system is required. However, in the case of wind energy conversion system (WECS), detailed models of the control system of the wind turbine generators (WTGs) are generally not available due to industry secrecy and confidentiality. The WECS system is generally assumed as 'black or grey- box' since no or limited information about the internal control dynamics is available from the vendors. Due to this lack of availability, an analytical impedance model for the WECS cannot be obtained with good accuracy. One can argue that it would be enough to measure the impedance of the inverter and then apply the Generalized Nyquist Criterion (GNC) on the measured source-load impedance and this can be true for a grid-tied inverter [7]. However, in the case of offshore wind farm's applications, the system has multiple wind power inverters which are powered by the HVDC system rather than a strong ac grid and the aggregated impedance frequency responses of the wind farms can only be obtained from measurement if the interconnected system of wind farms and HVDC transmission operates stably. In a real world application, there is no guarantee that the system will operate stably unless adequate stability measures have been taken before installation. Therefore, to ensure stable operation, it is necessary to assess the stability of the interconnected system analytically before connecting to the grid and during operation, as conditions may change and affect the stability [14]-[20]. In order to evaluate the stability analytically before connecting to the main grid, it is necessary to have a continuous transfer function for the analytical formulation of the impedance model assumed as grey-box WECS. For a continuous monitoring of stability and impedance re-shaping, it will be essential to estimate which are the most critical controller parameters of the inverters that participate in the observed oscillation. Based on this information, interaction phenomena between the controllers of the HVDC rectifier and wind power inverters can

Manuscript received July 5, 2017; revised November 9, 207, February 24, 2017 and April 17, 2018; accepted May 12, 2018. This work was supported in part by the project Protection and Fault Handling in Offshore HVDC Grids (ProOfGrids), managed by SINTEF Energy Research and financed by the Norwegian Research Council together with industry partners; EDF, NVE, National Grid, Siemens, Statkraft, Statnett and Statoil.

M. Amin is with the Department Electrical and Computer Engineering, Illinois Institute of Technology, Chicago, Illinois, USA. (e-mail: mohammad.amin@ieee.org).

M. Molinas is with the Department of Engineering Cybernetics, Norwegian University of Science and Technology, Trondheim-7491, Norway. (e-mail: marta.molinas@ntnu.no).

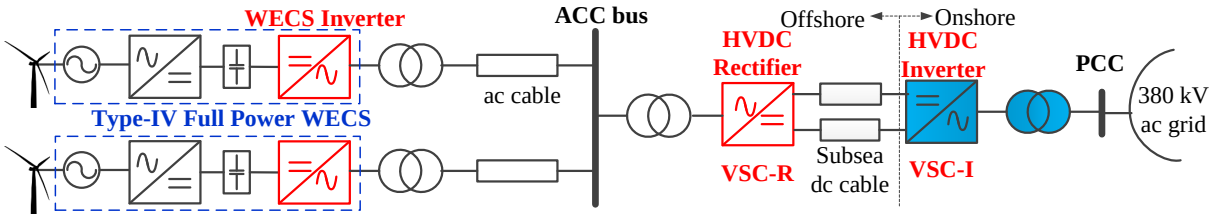

Fig. 1: Interconnected system of wind farms and VSC-based HVDC system.

be mitigated [2], [4].

In the literature, different methods for parameters and state estimation have been presented when detailed analytical models are known [21]-[22]; however, in the case of WECS, such models are generally not available due to industry secrecy. A method that can extract critical controller parameter easily accessible from measurement is very appealing in this case. To the authors' knowledge, estimation of controllers parameters of a WECS inverter based on impedance measurements has not been reported in the literature. This paper proposes such method for estimating the WECS inverter controllers' parameters from impedance field measurements. The proposed method is based on a grey-box model, i.e., a model that is based both on measurement and on some knowledge of the underlying system. The parameters to be estimated have a physical meaning within the assumed control structure of the WECS inverter. More broadly, the problem aiming at identifying the control parameters is an inverse problem, as it aims to compute the grey-box model parameters that gives rise to the measured impedance.

The contribution of the paper to the state-of-the-art comprises the following:

- A stability analysis method for HVDC connected wind farms based on a non-parametric impedance model.
- A method to extract the internal control dynamics of the WECS inverter based on a 'grey box' model using system identification techniques.
- Discussion on the role of the ratio between the bandwidths of the phase-locked-loop (PLL) and the HVDC rectifier control-loop, as one of the root causes of instability and important factor when re-shaping the impedances to guarantee the stability.

An example of a real-world application of this method is given here. A Grid Company is going to install an interconnected system of wind farms and HVDC system as shown in Fig. 1. Before installing this system, the Grid Company will perform thorough studies investigating the operation and stability. The Grid Company will need to simulate this system in a simulation tool like MATLAB/Simulink, PSCAD/EMTDC, or similar. The Grid Company will need a simulation model. For accurate analysis, Grid Company will get the simulation model from a selected Wind Turbine Generator Provider (WTGP). The Grid Company will also get an HVDC transmission system model from a selected HVDC transmission system provider (HVDC-TSP). The simulation models of the HVDC converter and WECS controller will be a black or grey-box model since no information regarding the control will likely be provided by the vendors due to confidentiality and industry secrecy. The Grid Company has now WECS model and HVDC system model from the WTGP and HVDC-TSP where both the WECS model and HVDC model are grey-box models. The Grid Company can now simulate the system. The Grid Company can analyze the stability of the system based on the method presented in this paper. Since it is an integration of multi-vendor components, it could be common to have some instability problem, due to unexpected interactions, since the interconnection has not been tested a priori. Therefore, if the Grid Company finds the interconnected system unstable, they should know, which component is causing the instability phenomena. However, not having access to details in a black/grey box model interconnection, will make it difficult to identify the cause. It is precisely here that the method presented in this paper will be able to tell with some certainty which component is causing the instability. If the Grid Company knows the cause of the instability, they can advise either the WTGC or the HVDC-TSP to redesign or re-tuned the control system. This paper provides a method for the Grid Company to assist in coping with this instability problem. This is just one example of the possible application of the method presented in this paper which there is no need of experimental trials.

The rest of the paper is organized in the following. Section II discusses the interconnected system configuration and the simulation results. Section III shows the stability analysis of the interconnected system based on the non-parametric impedance-based method. Section IV presents the method to extract the internal control dynamics of the inverter from the measurement data. Section V discusses the interaction analysis between the interconnected converters controllers based on the impedance-based method. Section VI presents the instability mitigation method by reshaping the impedance by re-tuning the control-loops bandwidth. Finally, the study concludes in Section VII.

II. Interconnected System Configuration, Control and Simulation

The interconnected system under study is depicted in Fig. 1. The system has two parts. The left part of the ac collection (ACC) bus is the offshore wind farm and the right part is the HVDC system.

A. Wind Farms Configuration and Control

The wind farms shown in Fig. 1 are connected to the ACC bus through a transformer and undersea cable. The WTGs are assumed to be a type-IV back-to-back WECS. Each wind

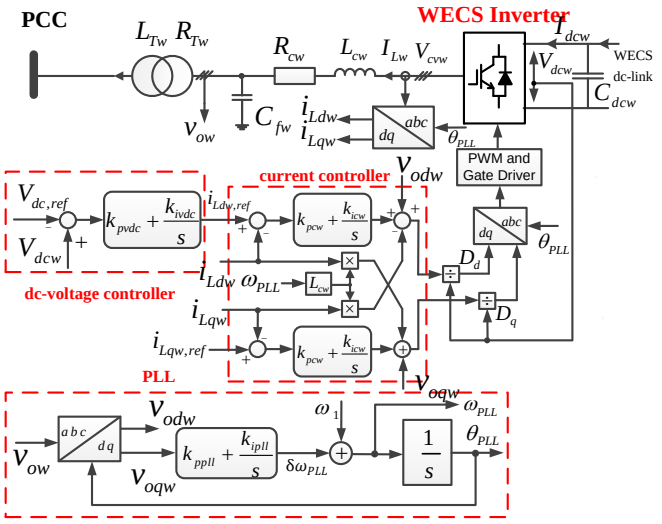

Fig. 2: Control structure of WECS inverter, WECS-I.

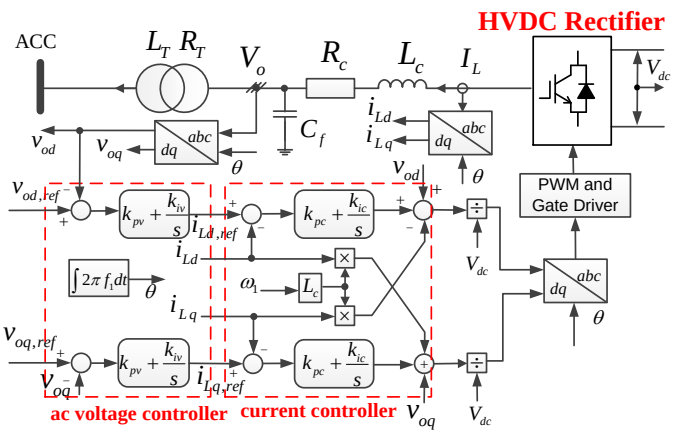

Fig. 3: Control structure of HVDC rectifier, VSC-R.

TABLE I: The VSC-HVDC system parameters

Parameter	Value	Parameter	Value
Rated Power, S_b	500 MVA	L_c	0.08 pu
Rated ac voltage	220 kV	R_c	0.00285 pu
Trans. inductance	0.1 pu	C_f	0.074 pu
Trans. resistance	0.01 pu	V_{dc}	360 kV

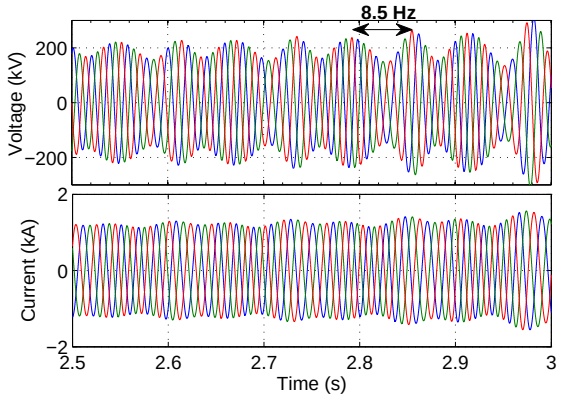

Fig. 4: Unstable case: Three phase voltages and currents at ACC bus.

farm is assumed to have 50 turbines with 3 MW rating each. To simplify the system model, 2x50 turbines are lumped into one unit of WTG with same generation capacity as the wind farms. The generator side VSC (WECS rectifier) regulates the power of the wind turbine based on the predicted wind speed and maximum power point tracking. The ac grid side VSC (WECS-I) regulates the dc link voltage of the WECS and reactive power. The control structure of the WECS-I is shown in Fig. 2 which has an inner-loop current control in synchronous reference frame. The d-axis current reference is obtained from the outer-loop dc voltage controller and the q-axis current reference is set according to the reactive power demand. A PLL is used to track the offshore grid frequency and synchronize with the ac collection bus voltage. The detailed on this control can be found in [2],[4], which will not be discussed in detailed due to page limit.

B. HVDC System Configuration and Control

The HVDC system consists of converter transformers, offshore HVDC rectifier (VSC-R), sub-sea dc cable, and grid-side onshore HVDC inverter (VSC-I). The VSC-HVDC system has a capacity of 500 MVA equivalent. The VSC-R is connected to the offshore ACC bus through a transformer with the same rating as the converter. The VSC-I is connected to the point common coupling (PCC) bus of 380 kV onshore ac grid through a 220/380-kV, 50-Hz, 500-MVA transformer. The HVDC-link dc voltage is 360 kV and the length of the dc line is 100 km.

The VSC-R behaves as a voltage source to the ac terminal and regulates the offshore ac voltage and frequency, while the VSC-I regulates the HVDC-link dc voltage and the reactive power. The control structure of the VSC-R is shown in Fig. 3. The detailed analytical modeling and control of VSC-based HVDC transmission system for the offshore wind farms integration has been presented in [2],[4] which has been adopted in this work and will not be discussed in detailed due to page limit.

C. Interconnected System Simulation Study

The interconnected system of the wind farm and HVDC transmission system has been implemented in MATLAB/Simulink association with SimPower System Block-set. The electrical circuit parameters of the HVDC system are given in Table I. The current-controller of the VSC-R is tuned at $H_{cc}(s) = 0.6366 + 14.25/s$ in pu with 90 degrees phase margin at 400 Hz crossover frequency. The ac voltage control-loop is tuned at $H_{vac}(s) = 0.09 + 40/s$ with 37 degree phase margin at 80 Hz crossover frequency. The switching frequency of HVDC VSC is 2 kHz. The ac voltage control-loop bandwidth is around 5 times lower than the inner-loop current controller and that satisfies the standard bandwidth ratio design criterion [23]. Therefore, the HVDC system is expected to operate stably.

A time domain simulation has been carried out and the resulting time domain responses are shown in Fig. 4. The

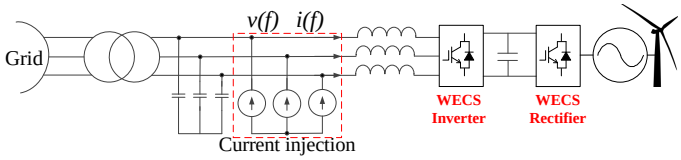

Fig. 5: Impedance measurement set up from the wind turbine generator.

system is unstable in the time domain simulation even when all the parameters and controllers satisfy the standard modeling and tuning criteria. As can be seen in Fig. 4, the voltages and currents have an oscillation with a frequency around 8.5 Hz and are increasing exponentially in amplitude.

One can assume that the instability is caused by (i) imperfect control tuning and modeling of the HVDC system and wind farms or (ii) interaction between the controls of wind farms and HVDC system [2],[4]. The first assumption can be checked by disconnecting the wind farms from the HVDC system and simulation can be carried out separately by connecting a simple $R-L$ load or constant power load (CPL) with the HVDC system and an ac grid with the wind farms [4]. Thus, a CPL with the same rated power of the wind farm has been connected to the HVDC system and a time domain simulation has been carried out. The system is found to be stable from the time domain simulation; therefore the HVDC system is itself stable for this tuning. Then, the wind farm has been connected to a strong ac grid and the time domain simulation confirms that the wind farm operates stably without the HVDC system. By way of this verification, it can be concluded that the instability is resulting from the control interaction of the HVDC rectifier VSC-R and wind power inverter WECS-I [2],[4].

III. Non-parametric Impedance Identification and Grey-box Model

This section presents a method to study the stability analysis based on a non-parametric impedance.

A. Identification of Impedance Model of WECS-I

The basic assumption for the impedance identification is that the WTGs will be identical in structure and control from a vendor. A single WTG has been connected to the main ac grid without the HVDC transmission line and the impedance frequency responses have been measured from 1 Hz to 5 kHz with 75 measurement points in dq-frame. The measurement set-up is shown in Fig. 5. A perturbation current of 5% of rated current at different frequencies is applied as shown in Fig. 5. The impedances are referred to a dq-synchronous reference frame and they are represented as a 2x2 matrix, therefore, two sets of linear independent perturbation signals are applied separately. The perturbation is in dq-domain. The perturbation is transformed to the sequence domain using inverse Park Transform in order to be compatible with the injection structure. Both the voltages and the currents are measured. The measured signals are in sequence domain, however, the impedances are in dq-domain. Therefore, the

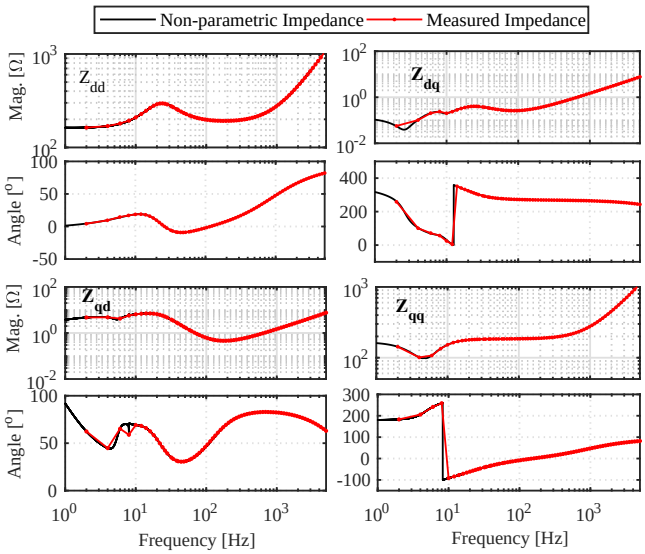

Fig. 6: Impedance frequency responses of the WECS (Solid line is from the system identification and the dot-line is from measurement).

voltages and currents signal are transformed back to dq-domain using Park Transform. The Fast Fourier Transform (FFT) tool from SimPower System is used to analyze the different harmonic voltage and current. The impedance is calculated by dividing the voltage by current at each frequency [24], [25]. The measurement point has been selected randomly in logarithmic scale. More measurement points will give a better approximation of the impedance model. A system identification technique (SIT) [26] has been used to estimate the transfer function of the non-parametric impedance matrix in dq-domain and can be expressed by

$$\mathbf{Z^{dq}_{WECS-I-SIT}}(s) = \begin{bmatrix} Z^{dd}_{WECS-I-SIT}(s) & Z^{dq}_{WECS-I-SIT}(s) \\ Z^{qd}_{WECS-I-SIT}(s) & Z^{qq}_{WECS-I-SIT}(s) \end{bmatrix}. \quad (1)$$

The elements of the non-parametric impedance matrix, for example, $Z^{dd}_{WECS-I-SIT}(s)$ is defined as

$$Z^{dd}_{WECS-I-SIT}(s) = \frac{b_m s^m + b_{m-1}s^{m-1} + ... + b_o}{a_n s^n + a_{n-1}s^{n-1} + ... + a_o} \quad (2)$$

where b_m, b_{m-1},...b_o, a_n, a_{n-1},...a_o are constant coefficients and m and n are the order of Zero and Pole of the impedance model. Detailed discussion on the SIT is omitted here, however, the reader can follow the literature for more details in [26]-[28]. The order of the transfer function is not dependent on the control strategy. If we increase the order of the transfer function it will increase the computational complexity and on the other hand, if we reduce the order, the accuracy of the estimated transfer function will be compromised. It is a trade-off between computational complexity and accuracy of the transfer function estimation. The order of the transfer function is selected (7 in this case) such that the error between the measurement and the model identification is less than 0.10%. Fig. 6 shows the identified impedance frequency responses

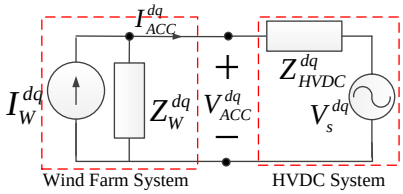

Fig. 7: Impedance based equivalent model of offshore ac grid system

with the system identification applied the measured impedance by point-by-point simulation. As can be seen, the obtained transfer function of the impedance model has a very good agreement with measured impedance frequency responses in both magnitude and phase.

B. Stability Analysis based on Non-parametric Impedance

The small-signal impedance model of the interconnected system of Fig. 1 is shown in Fig. 7 where $\mathbf{Z^{dq}_{HVDC}}$ and $\mathbf{Z^{dq}_{W}}$ are the total impedance of the HVDC system and the wind farm seen from the offshore ACC point, respectively. Note that the impedances are in dq-domain and are 2x2 matrices. The bold font is used to represent in a matrix form. In order to calculate the total impedance from the ACC point, all impedances are converted to dq-domain using the same system transformation angle. The $\mathbf{Z^{dq}_{HVDC}}$ can be expressed by

$$\mathbf{Z^{dq}_{HVDC}}(s) = \mathbf{Z^{dq}_{T}}(s) + \left(\left(\mathbf{Z^{dq}_{VSC-R}}(s)\right)^{-1} + \left(\mathbf{Z^{dq}_{Cf}}(s)\right)^{-1}\right)^{-1} \quad (3)$$

where $\mathbf{Z^{dq}_{VSC-R}}(s)$, $\mathbf{Z^{dq}_{T}}(s)$ and $\mathbf{Z^{dq}_{Cf}}(s)$ are the dq-impedance of the HVDC rectifier VSC-R, HVDC converter transformer and the capacitive filter, respectively. The analytical impedance model of the HVDC rectifier is given by [4]

$$\mathbf{Z^{dq}_{VSC-R}}(s) = -\left(\mathbf{I} - V_{dc}\mathbf{G_{pwm}}(s)\left(\mathbf{I} - \mathbf{G_{ccR}}(s)\mathbf{G_{vR}}(s)\right)\right)^{-1} \left(\mathbf{Z_{0R}}(s) + V_{dc}\mathbf{G_{pwm}}(s)\left(\mathbf{G_{ccR}}(s) + \mathbf{Z_{del}}\right)\right) \quad (4)$$

where the elements of the impedance matrix are

$$\mathbf{Z_{0R}}(s) = \begin{bmatrix} R_c + sL_c & -\omega_1 L_c \\ \omega_1 L_c & R_c + sL_c \end{bmatrix};$$

$$\mathbf{Z_{del}} = \begin{bmatrix} 0 & \omega_1 L_c \\ -\omega_1 L_c & 0 \end{bmatrix};$$

$$\mathbf{G_{ccR}}(s) = \begin{bmatrix} k_{pc} + k_{ic}/s & 0 \\ 0 & k_{pc} + k_{ic}/s \end{bmatrix};$$

$$\mathbf{G_{vR}}(s) = \begin{bmatrix} k_{pv} + k_{iv}/s & 0 \\ 0 & k_{pv} + k_{iv}/s \end{bmatrix};$$

$$\mathbf{G_{pwm}}(s) = \begin{bmatrix} H_{pwm}(s) & 0 \\ 0 & H_{pwm}(s) \end{bmatrix};$$

$$H_{pwm}(s) = e^{-sT_s}\frac{1 - e^{-sT_s}}{sT_s};$$

and $H_{pwm}(s)$ models the PWM delays, T_s represents the sampling delay, and $\mathbf{I}$ is a 2x2 identity matrix.

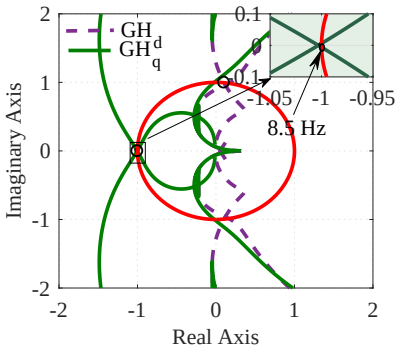

Fig. 8: Characteristics loci of the minor-loop gain (Red line is the unit circle).

The impedance of the wind farms from the ACC point can be given by

$$\mathbf{Z^{dq}_{W}}(s) = \frac{1}{n}\Big(\mathbf{Z^{dq}_{ac-cable}}(s) + \mathbf{Z^{dq}_{Tw}}(s) + \left(\left(\mathbf{Z^{dq}_{WECS-I-SIT}}(s)\right)^{-1} + \left(\mathbf{Z^{dq}_{Cfw}}(s)\right)^{-1}\right)^{-1}\Big) \quad (5)$$

where $\mathbf{Z^{dq}_{ac-cable}}(s)$, $\mathbf{Z^{dq}_{Tw}}(s)$ and $\mathbf{Z^{dq}_{Cfw}}(s)$ are the dq-impedance of the ac cable, WECS transformer and the capacitive filter, respectively; n is the number of wind farms.

If the WTGs are from different vendors, the control structure could be different. Hence, it will be necessary to obtain the transfer function of the impedance frequency responses for the different vendor's WTGs by applying the SIT and the aggregated non-parametric impedance model needs to be obtained for wind farms with different control structure to study the stability of the interconnected system.

Based on the representation in Fig. 7, the response of the ACC bus voltage can be written by (6).

$$\mathbf{V^{dq}_{ACC}}(s) = \left(\mathbf{V^{dq}_{s}}(s) + \mathbf{Z^{dq}_{HVDC}}(s)\mathbf{I^{dq}_{W}}(s)\right)\left(\mathbf{I} + \left(\mathbf{Z^{dq}_{HVDC}}(s)\right)\left(\mathbf{Z^{dq}_{W}}(s)\right)^{-1}\right)^{-1} \quad (6)$$

For system stability studies, it is assumed that (i) the ac voltage of VSC-R is always stable when unloaded; and (ii) the wind farms current is stable when it is connected to a stable source. Therefore, the stability of the interconnected system depends on the second term of the right-hand side of (6) and the ACC bus voltage will be stable if and only if the impedance ratio matrix, $\left(\mathbf{Z^{dq}_{HVDC}}(s)\right)\left(\mathbf{Z^{dq}_{W}}(s)\right)^{-1}$ which can be defined as the minor loop gain of the feedback control system as

$$\mathbf{G}(s)\mathbf{H}(s) = \left(\mathbf{Z^{dq}_{HVDC}}(s)\right)\left(\mathbf{Z^{dq}_{W}}(s)\right)^{-1} \quad (7)$$

meets the Nyquist Stability Criterion [1], [5].

The impedance matrices of (7) are known, hence, the stability of the entire system can now be effectively determined analytically before connecting to the grid since all the parameters are now available for stability analysis. Fig. 8 shows the frequency domain stability analysis results for the simulation presented in the previous section. As can be seen in Fig. 8,

the q-axis impedance dominated characteristics loci encircles the point (-1, j0) at frequency 8.5 Hz and there is a pole in the right half-plane (RHP), therefore, the system has become unstable.

To obtain aggregated equivalent impedance of the wind farm, it has been assumed that all the WTGs are operating in the same steady-state point. In the real case, the operating point might not be the same for all WTGs, therefore, it is essential to check the stability of the interconnected system for different operating point of the WTGs.

IV. Extraction of WECS Inverter Controllers' Parameters

This Section presents the method to reveal the internal dynamics of the WECS inverter from the identified non-parametric impedance frequency response to identify which controller is participating in the observed oscillation while the WECS is considered to be a grey-box. The main assumption here is that the control structure is of the same form as in Fig. 2. It has been observed by analyzing last five year's literature on the control of type IV full power WECS that more than 80% of the grid side converter control in the WECS is based on the vector control as shown in Fig. 2. Though, it is yet unknown how much the percentage of which control system used by the industrial level, the presented method will reveal this secrecy by applying the method to a WECS from different vendors.

The analytical impedance model of the WECS inverter has been derived as discussed in [4]. The analytical model is equivalent to the model obtained by the system identification technique and can be expressed as a function of controller parameters by

$$\mathbf{Z^{dq}_{WECS-I-SIT}}(s) = \left(\mathbf{I} - V_{dc}\mathbf{G_A^{-1}G_C} + \mathbf{G_D G_{vd} G_A^{-1} G_C}\right)^{-1} \left(-\mathbf{Z_{0w}} - \mathbf{G_D G_{vi}} + (V_{dc}\mathbf{I} - \mathbf{G_D G_{vd}})(\mathbf{G_A^{-1} G_B})\right) \quad (8)$$

and the elements of the impedance matrix are given in Appendix. The impedance model in (8) is in dq-frame and a 2x2 matrix. The diagonal elements of (8) can be written as

$$Z^{dd}_{WECS-I-SIT}(s) = \frac{Z_0(s) + \frac{D_d^2}{sC_{dc}} + \left(V_{DC} - \frac{D_d I_d}{sC_{dc}}\right)\frac{Z_0(s)\psi_n(s)}{\psi_d(s)}}{1 - \left(V_{DC} - \frac{D_d I_d}{sC_{dc}}\right)\frac{H_{pwm}(s)}{\psi_d(s)}} \quad (9a)$$

$$Z^{qq}_{WECS-I-SIT}(s) = \frac{Z_0(s) + \frac{D_q^2}{sC_{dc}} + G_{cc-ol}(s)Z_0(s)}{1 - V_{DC}H_{pwm}(s) - G_{PLL}(s)\psi_{PLL}(s)} \quad (9b)$$

where

$$\psi_n(s) = (D_d G_{vdc-ol}(s)(1 + G_{cc-ol}(s)) + G_{cc-ol}(s))$$
$$\psi_d(s) = 1 + I_d Z_o(s) G_{vdc-ol}(s)(1 + G_{cc-ol}(s))$$
$$\psi_{PLL}(s) = G_{cc-ol}(s)Z_0(s)I_d - V_{DC}H_{pwm}(s)V_d + V_{DC}D_d$$
$$G_{cc-ol}(s) = H_{pwm}(s)\left(k_{pcw} + k_{icw}/s\right)/Z_0(s)$$
$$G_{cc-cl}(s) = G_{cc-ol}(s)/(1 + G_{cc-ol}(s))$$
$$G_{vdc-ol}(s) = \left(k_{pvdc} + k_{ivdc}/s\right)G_{cc-cl}(s)/(sC_{dc})$$
$$G_{PLL}(s) = \left(k_{ppll} + k_{ipll}/s\right)/\left(s + V_{od}\left(k_{ppll} + k_{ipll}/s\right)\right)$$

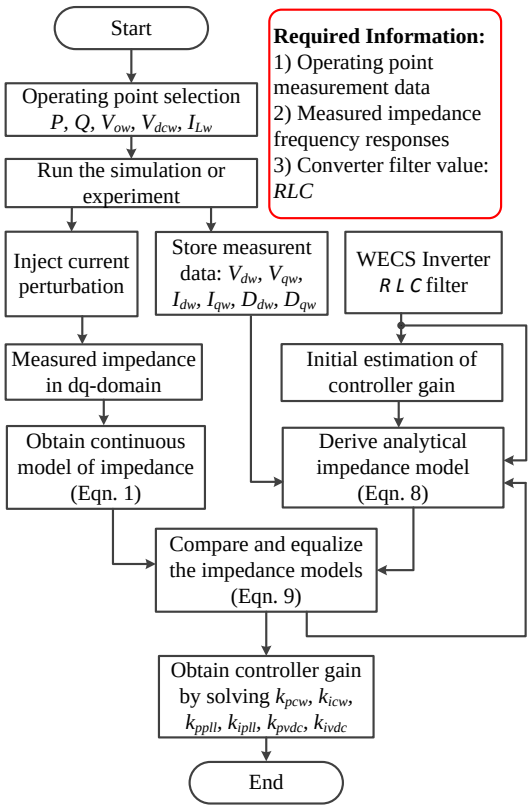

Fig. 9: Illustration of controller gain extraction method from measured impedance for dq-control.

and $G_{cc-ol}(s)$ and $G_{vdc-ol}(s)$ are the open-loop transfer function of the current and dc voltage control-loop, respectively, $D_d = V_{cvdw}/V_{dcw}$ and $D_q = V_{cvqw}/V_{dcw}$ are modulation index at operating point, and $Z_0(s) = R_{cw} + sL_{cw}$.

In (9), all the elements are known from the measurement data except the proportional and integral gain of the current controller (k_{pc}, k_{ic}), dc voltage controller (k_{pvdc}, k_{ivdc}) and the PLL (k_{ppll}, k_{ipll}). The inverse problem consists of two equations with six unknown variables. In order to solve these equations, (9) is represented in $j\omega$-domain and the required number of equations can be obtained at different frequencies from measurement data and by separating them in real and imaginary part. Now, solving those equations by iteration, all controllers gains are obtained. The bandwidth extraction method is presented through a flow chart as shown in Fig. 9.

In this paper, the method is presented for the decoupled d-q frame control of a WECS VSC as an example of controller bandwidth estimation, however, this procedure can be applied to other type of controllers of the VSC to extract the controller dynamics. In a real world application, we will not know which control method is implemented in the VSC, however, the impedance frequency response would be different based on the implemented control. An example of the impedance frequency responses of the WECS system for two different control strategies has been discussed in [29]. One is based on the dq-frame control and the other is the synchronverter control [29], [30]. The impedance frequency responses are different for the different control strategies which enable the estimation

of the controller dynamics even when the control strategy is unknown. In order to identify controller dynamics for other type of converter control and to generalize the extraction method, few steps have to be followed. First, the analytical expression of the impedance model of the VSC for different control methods (as given in (9) for dq-control method) needs to be derived. And then the analytical impedance model and the measured impedance are equalized. Finally, the equations are solved to estimate the control dynamics as illustrated in Fig. 9.

The methodology presented in this paper is equally applicable to multi-vendor WECS. A single vendor is assumed in this paper to make the idea easier to understand. In order to determine the stability of an interconnected systems of multi-vendors WECS and HVDC system, the impedance transfer functions have to be obtained by measurement for all vendors WECS using system identification technique. Obtaining the impedance transfer functions by system identification remain the same regardless of the vendor. The vendor does not need to disclose sensitive information about the internal controllers. Only a black-box model will be required. The stability of an interconnected system having WECS from multi-vendors can be determined by obtaining impedance transfer functions for the WECS from different vendors as presented in this paper. Finally, the total impedance of the wind farm can be obtained from the ac collection bus. After having the impedance model, the generalized Nyquist stability criterion can be used to determine the stability of the interconnected system of HVDC connected wind farms from multi-vendors.

V. Impedance-based Interaction Analysis

In order to identify which controller is participating in the observed oscillation, the diagonal elements of the VSC-R and WECS-I impedance are mainly focused since the diagonal elements are dominating along the entire Nyquist path [4].

The diagonal elements of the VSC-R impedance from (4) can be written by

$$Z^{dd}_{VSC-R}(s) = Z^{qq}_{VSC-R}(s) = \frac{1}{G_{cc-cl,R}(s)H_{vac}(s)} \quad (10)$$

where $H_{vac}(s)$ is the ac voltage PI controller transfer function, $H_{vac}(s) = k_{pv} + k_{iv}/s$; $G_{cc-cl,R}(s)$ is the closed-loop transfer function of the current control-loop and can be written as

$$G_{cc-cl,R}(s) = \frac{V_{dc}H_{pwm}(s)H_{cc}(s)/\left(R_c + sL_c\right)}{1 + V_{dc}H_{pwm}(s)H_{cc}(s)/\left(R_c + sL_c\right)} \quad (11)$$

and the PI current controller transfer function, $H_{cc}(s) = k_{pc} + k_{ic}/s$. Including the filter capacitor, the diagonal elements can be expressed as a function of the ac voltage control-loop as

$$Z^{dd}_{VSC-R}(s) = Z^{qq}_{VSC-R}(s) = \frac{1}{sC_f(G_{vac-ol}(s) + 1)} \quad (12)$$

where $G_{vac-ol}(s)$ is the open-loop transfer function of the ac voltage control-loop and can be given by

$$G_{vac-ol}(s) = H_{vac}(s)G_{cc-cl,R}(s)\frac{1}{sC_f}. \quad (13)$$

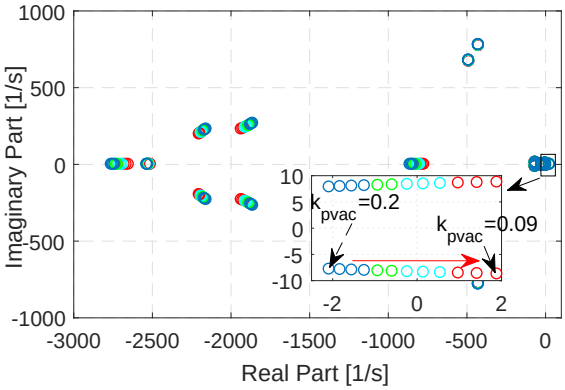

Fig. 10: Trajectory of eigenvalue for a change of proportional gain of ac voltage controller of the HVDC rectifier.

From (12), it can be seen that the diagonal elements of HVDC rectifier impedance depend on the open-loop transfer function of the ac voltage controller. The higher the control bandwidth of the ac voltage control-loop is, the lower the impedance magnitude of the HVDC converter. Moreover, the diagonal elements of the impedance are equal in magnitude and do not depend on the operating point.

The diagonal elements of WECS-I impedance in (9) indicate that Z_{dd}-impedance of the WECS-I depends on the outer-loop dc voltage controller, inner-loop current controller and operating point. Z_{qq}-impedance depends on the closed-loop PLL bandwidth, inner-loop current controller and the operating point.

The passive components such as the inductor, capacitor and resistor have an equal impact on both the d- and q-axis impedance, however, the controllers in the wind farm inverters are different since d-axis has outer-loop dc voltage control while the q-axis has PLL synchronization loop. As can be seen in Fig. 8, the d-axis impedance dominated Nyquist plot has sufficient phase margin and is far from the stability marginal point while the Nyquist plot of the q-axis dominated impedance encircles the point (-1, j0). Thus the controllers in the q-axis are interacting resulting in instability in the interconnected areas. The HVDC rectifier's most outer control in the q-axis is the ac voltage control-loop and the wind farms inverter's most outer controller in the q-axis is the PLL. The controllers in VSC-R and WECS-I with the slowest bandwidth are the dominating part in the impedance magnitude at low frequencies, therefore the ac voltage controller of the HVDC rectifier and the PLL of WECS-I are interacting resulting in instability.

To confirm the instability resulting in the interaction of the ac voltage controller of the HVDC rectifier and WECS inverter, a state-space model has been derived for the system and the system eigenvalues have been calculated analytically. A trajectory of eigenvalue plot for variation of ac voltage controller proportional gain is shown in Fig. 10. As can be seen, the system has an unstable complex conjugate eigenvalue at $1.9 \pm j2\pi 8.5$ with an oscillation frequency of 8.5 Hz for $k_{pv} = 0.09$. This is the unstable case that is observed in the time domain simulation shown in Fig. 4 and frequency domain

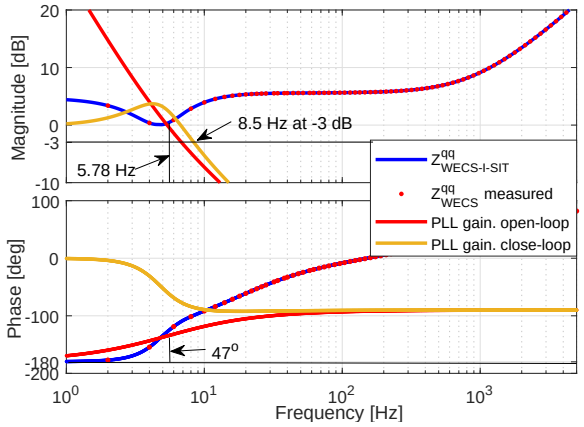

Fig. 11: Loop-gain of the PLL and Z_{qq} impedance of the WECS inverter.

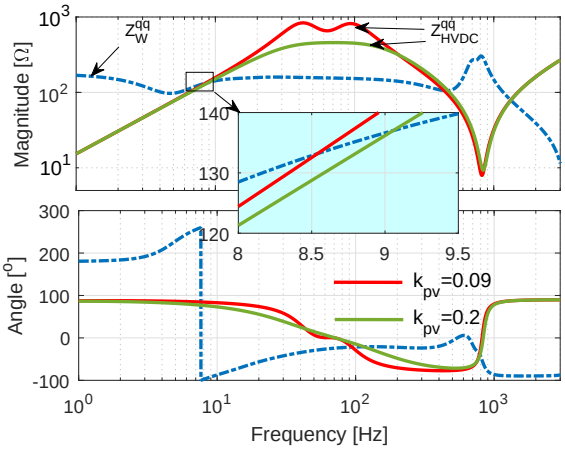

Fig. 12: Z_{qq}-impedance of the wind farms and the HVDC system for two cases of ac voltage controller tuning.

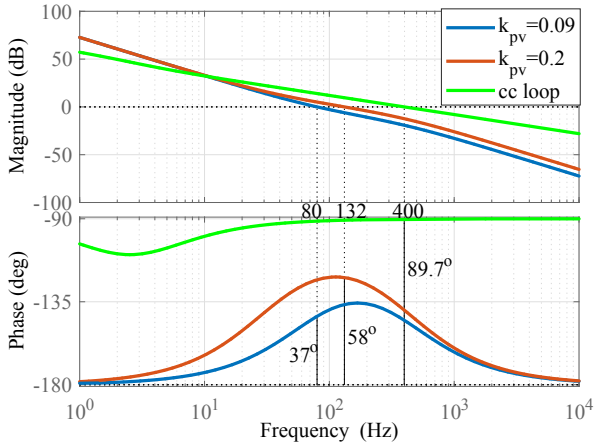

Fig. 13: Control-loop gain of the ac voltage controller for different value of k_{pv} and the current controller (cc loop) of the HVDC rectifier.

analysis shown in Fig. 8. The participation factor analysis has been carried out for the unstable eigenvalues to identify the contribution of the states. From the participation factor analysis, it is found that the PLL and the ac voltage controller are the most contributing states for the unstable eigenvalue. The participation factor analysis proves that the instability is caused by the interaction of the ac voltage controller and the PLL which gives the same conclusion as the presented impedance-based method.

VI. Instability Mitigation Method

The bandwidth information of the PLL of the WECS-I is extracted using this method. Fig. 11 shows the frequency response of the control-loop gain of the PLL. The open-loop gain of the PLL has a phase margin 47 degrees at 5.78 Hz and the closed-loop has a bandwidth around 8.5 Hz. Moreover, Fig. 11 also shows the Z_{qq}-impedance of the WECS inverter from the SIT and numerical simulation. As can be seen, the impedance has a resonance at low frequency around 5 Hz which indicates crossover frequency of the PLL open-loop gain. The bandwidth is calculated at -3dB magnitude, therefore if we move forward 3 dB more from resonance point, the frequency is found 8.5 Hz which is the closed-loop bandwidth of the PLL.

Fig. 12 shows the impedance frequency responses of the wind farm and the HVDC system from ac collection point. The HVDC rectifier impedances are shown for two cases with proportional gain 0.09 and 0.2 of the ac voltage controller. Since the system becomes unstable only for the q-axis impedance, Z_{qq}-impedance is of most interest. Z_{qq}-impedance of the HVDC rectifier behaves as inductive up to a frequency around 40 Hz and it becomes a band pass filter at frequency of the ac voltage control-loop bandwidth. However, Z_{qq}-impedance of the wind farm behaves capacitive as up to the crossover frequency of the PLL-loop and shows the characteristics of band reject filter. As can be seen in Fig. 12, Z_{qq}-impedance of the wind farm intersects the HVDC impedance at 8.5 Hz for ac voltage-controller proportional gain 0.09. It is observed that the system becomes unstable if Z_{qq}-impedance magnitude of the HVDC system becomes larger than the wind farm impedance magnitude at the frequency below the bandwidth of the PLL. In order to avoid the interaction between the ac voltage controller of VSC-R and WECS-I PLL, the controls of the both VSCs need to be re-tuned in such a way that Z_{qq}-impedance magnitude of the HVDC system is kept lower than Z_{qq}-impedance magnitude of the wind farm at the frequency of the PLL bandwidth.

Based on (12), the higher bandwidth of the ac voltage controller of the HVDC VSC-R reduces impedance magnitude of the HVDC system. Initially, the ac voltage controller bandwidth (80 Hz) of VSC-R was five times lower than the inner-loop current controller bandwidth (400 Hz). A standard practice for the converter designer is that the outer-loop bandwidth should be three to ten times smaller than the inner control loop [23]. Therefore, in a first attempt, the bandwidth of the ac voltage control loop has been increased. The ac voltage controller proportional gain is increased to 0.2 and the control-loop phase margin is 58 degrees with 132 Hz crossover frequency while previously the crossover frequency was 80 Hz. Fig. 13 shows the control-loop frequency response for

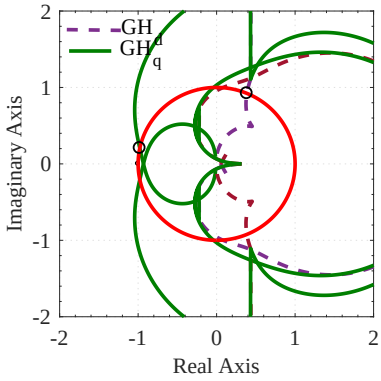

Fig. 14: Characteristics loci of minor-loop gain for re-tuning of the ac voltage controller of the HVDC rectifier (Red line is the unit circle).

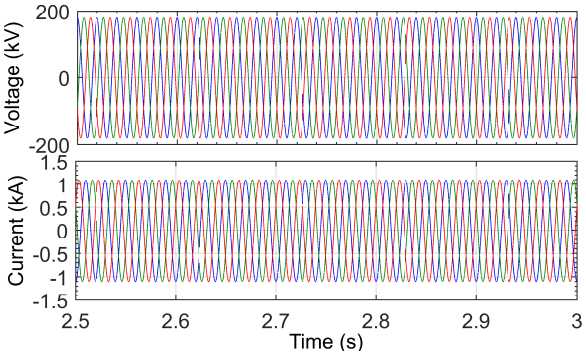

Fig. 15: Three phase voltages and currents at ACC bus after ac voltage control re-tuning.

the two cases of ac voltage control-loop tuning of the HVDC rectifier. For this re-tuning of the ac voltage controller, the bandwidth of the ac voltage controller becomes three times smaller than the inner current control loop. The impedance frequency responses is shown in Fig. 12 for this ac voltage tuning. As can be seen in Fig. 12, Z_{qq}-impedance of the wind farm intersects the HVDC impedance at around 9 Hz for the new tuning of the ac voltage-controller. Z_{qq}-impedance magnitude of the HVDC system becomes smaller than the impedance magnitude of the wind farm at the frequency below the bandwidth of the WECS-I PLL. Frequency domain stability analysis has been carried out for this new tuning of the ac voltage control of the HVDC VSC-R. Fig. 14 shows the frequency domain stability analysis results for this tuning. As can be seen, the loci plots do not encircle the point (-1, j0) and there is no pole in the RHP, hence the system will operate stably. To further verify the theoretical analysis, a time domain simulation has been carried out for the new control tuning of the ac voltage control loop while other control-loops bandwidth remain the same. Fig. 15 shows the time domain responses from the simulation. The system operates stably for this tuning.

It has been observed that if the PLL open-loop phase margin is more than 40 degrees and the PLL closed-loop bandwidth is 10 times smaller than the open-loop crossover frequency of the ac voltage controller, the system operates stably. Another

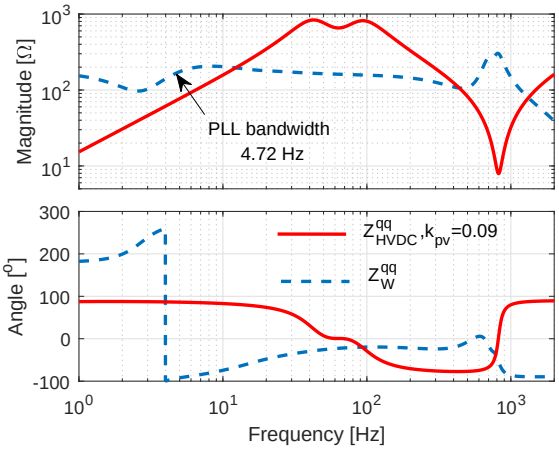

Fig. 16: Z_{qq}-impedance of the wind farms and the HVDC system for re-tuning the PLL.

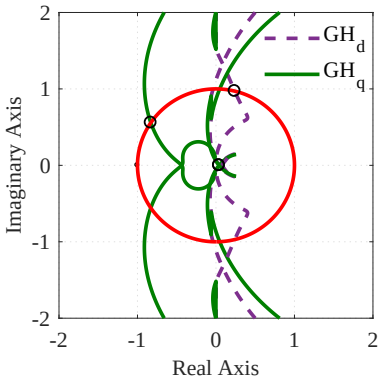

Fig. 17: Characteristics loci of minor-loop gain for re-tuning of WECS PLL (Red line is the unit circle).

example is shown that proves this observation by re-tuning the PLL loop-gain at 3.17 Hz crossover frequency with 42 degrees phase margin and the PLL closed-loop control bandwidth is 4.72 Hz for the unstable case of Fig. 8. Fig. 16 shows the impedance frequency responses of the wind farm from the ac collection point together with the HVDC impedance for new tuning of the PLL. As can be seen, Z_{qq}-impedance magnitude of the wind farms does not intersect the HVDC impedance at frequency below the cutoff frequency of the PLL-loop. Fig. 17 shows the Nyquist plot of minor-loop gain. As can be seen, the Nyquist plots do not encircle the point (-1, j0) and there is no pole in the RHP, the system operates stably. This frequency domain analysis has been further confirmed by a time domain simulation which is similar to the one shown in Fig. 15.

The observation complies with other works available in the literature [2], [4]. Table II presents a stability comparison for the different bandwidth of the PLL and ac voltage control-loop from different works. As shown, when PLL bandwidth (BW_{PLL}) is 10 times smaller than the ac voltage control-loop bandwidth of the HVDC rectifier BW_{HVDC}, the inter-connected system of wind farms and HVDC system is stable which complies with results presented in this work.

VII. Conclusion

The paper analyses the stability of an interconnected system of wind farms and HVDC transmission system based on a non-parametric impedance identified from measured impedance by applying a system identification technique. A grey-box method is proposed to estimate controllers parameters of WECS inverter from the measurements of frequency domain equivalent impedance. For this, the WECS is assumed to be a grey box when limited information is provided by the vendors due to confidentiality and industry secrecy. It is shown how with this method it is possible to identify which controller in the interconnected system has a major impact in the observed system oscillations. Based on this observation, a mitigation technique is proposed by reshaping the impedance of the subsystem re-tuning only the corresponding critical controller bandwidth of the interconnected converters. It is observed that the HVDC rectifier ac voltage controller's bandwidth should be ten times higher than the control bandwidth of the WECS inverter's PLL to ensure stability of the interconnected system by keeping the magnitude of the q-axis impedance of the HVDC system lower than the magnitude of q-axis impedance of the wind farm up to the bandwidth of the WECS inverter's PLL. The method presented has potential for immediate application in the wind industry based on the relevant information it offers with great simplicity e. g. impedance measurement based, minimal required information of WECS detail design parameters. The method presented in this paper can extract the controller parameters for the dq-frame control of the wind power inverter. Use of the method for more general purpose and other type of control of an inverter will be reported in a future work.

TABLE II: a comparison of bandwidth of the ac voltage control-loop and the PLL

References	BW_{HVDC}	BW_{PLL}	$\frac{BW_{HVDC}}{BW_{PLL}}$	Stability
This paper	80 Hz	8.5 Hz	9.5	Unstable
	132 Hz	8.5 Hz	15.5	Stable
	80 Hz	4.5 Hz	17	Stable
Ref. [2]	100 Hz	30 Hz	3.3	Unstable
	100 Hz	15 Hz	6.5	Stable
Ref. [4]	315 Hz	9 Hz	35	Stable
	336 Hz	9 Hz	37	Stable
	185 Hz	9 Hz	20	Stable

Appendix

Elements of the WECS inverter impedance matrix

$$\mathbf{G_A} = (\mathbf{I} + \mathbf{G_{pwm}}\mathbf{G_{cc}}\mathbf{G_{dc}}\mathbf{G_{vd}})$$
$$\mathbf{G_B} = \mathbf{G_{pwm}}\left(-\mathbf{G_{cc}} + \mathbf{Z_{del}} - \mathbf{G_{cc}}\mathbf{G_{dc}}\mathbf{G_{vi}}\right)$$
$$\mathbf{G_C} = \mathbf{G_{pwm}}\left(\left(-\mathbf{G_{cc}} + \mathbf{Z_{del}}\right)\mathbf{G^i_{PLL}} + \mathbf{G^v_{PLL}} - \mathbf{G_{cc}}\mathbf{G_{dc}}\mathbf{G_{vq}}\right)$$
$$\mathbf{Z_{0w}} = \begin{bmatrix} R_{cw} + sL_{cw} & -\omega_1 L_{cw} \\ \omega_1 L_{cw} & R_{cw} + sL_{cw} \end{bmatrix}$$
$$\mathbf{Z_{del}} = \begin{bmatrix} 0 & \omega_1 L_{cw} \\ -\omega_1 L_{cw} & 0 \end{bmatrix}$$
$$\mathbf{G_{cc}} = \begin{bmatrix} k_{pcw} + k_{icw}/s & 0 \\ 0 & k_{pcw} + k_{icw}/s \end{bmatrix}$$
$$\mathbf{G_{dc}} = \begin{bmatrix} k_{pvdc} + k_{ivdc}/s & 0 \\ 0 & 0 \end{bmatrix}$$
$$\mathbf{G_D} = \begin{bmatrix} D_d & 0 \\ D_q & 0 \end{bmatrix}$$
$$\mathbf{G_{vd}} = \begin{bmatrix} Z_{dcw} I_{Ld0w} & Z_{dcw} I_{Lq0w} \\ 0 & 0 \end{bmatrix}$$
$$\mathbf{G_{vi}} = \begin{bmatrix} Z_{dc} D_d & Z_{dcw} D_q \\ 0 & 0 \end{bmatrix}$$
$$Z_{dcw} = \frac{sL_{dcw} + R_{dcw}}{s^2 C_{dcw} L_{dcw} + sC_{dcw} R_{dcw} + 1}$$
$$\mathbf{G^i_{PLL}} = \begin{bmatrix} 0 & G_{PLL}(s) I_{Lq0w} \\ 0 & -G_{PLL}(s) I_{Ld0w} \end{bmatrix}$$
$$\mathbf{G^v_{PLL}} = \begin{bmatrix} 1 & G_{PLL}(s) V_{odw} \\ 0 & 1 - G_{PLL}(s) V_{odw} \end{bmatrix}$$
$$G_{PLL}(s) = \frac{k_{ppll} + k_{ipll}/s}{s + V_{odw}(k_{ppll} + k_{ipll}/s)}$$

References

[1] R. D. Middlebrook, Input filter considerations in design and application of switching regulators, in Rec.1976 IEEE Ind. Appl. Soc. Annu. Meeting, pp. 366382.

[2] H. Liu and J. Sun, "Voltage Stability and Control of Offshore Wind Farms With AC Collection and HVDC Transmission," IEEE J. Emerg. Sel. Topics Power Electron., vol.2, no.4, pp.1181,1189, Dec. 2014

[3] J. Lyu, X. Cai and M. Molinas, "Frequency Domain Stability Analysis of MMC-Based HVDC for Wind Farm Integration," IEEE J. Emerg. Sel. Topics Power Electron., vol. 4, no. 1, pp. 141-151, March 2016.

[4] M. Amin and M. Molinas, "Understanding the Origin of Oscillatory Phenomena Observed between Wind Farms and HVDC Systems," IEEE J. Emerg. Sel. Topics Power Electron., vol. 5, no. 1, pp. 378-392, March 2017.

[5] J. Sun, "Impedance-Based Stability Criterion for Grid-Connected Inverters," IEEE Trans. on Power Electron., vol.26, no.11, pp.3075,3078, Nov. 2011

[6] M. Cespedes, L. Xing and J. Sun, "Constant-Power Load System Stabilization by Passive Damping," IEEE Trans. on Power Electron., vol. 26, no. 7, pp. 1832-1836, July 2011.

[7] M. Cespedes and J. Sun, "Impedance Modeling and Analysis of Grid-Connected Voltage-Source Converters," IEEE Trans. on Power Electron., vol. 29, no. 3, pp. 1254-1261, March 2014.

[8] B. Wen, D. Dong, D. Boroyevich, R. Burgos, P. Mattavelli and Z. Shen, "Impedance-Based Analysis of Grid-Synchronization Stability for Three-Phase Paralleled Converters," in IEEE Trans. on Power Electron., vol. 31, no. 1, pp. 26-38, Jan. 2016.

[9] S. Lissandron, L. Dalla Santa, P. Mattavelli and B. Wen, "Experimental Validation for Impedance-Based Small-Signal Stability Analysis of Single-Phase Interconnected Power Systems With Grid-Feeding Inverters," IEEE J. Emerg. Sel. Topics Power Electron., vol. 4, no. 1, pp. 103-115, March 2016.

[10] W. Cao, Y. Ma, L. Yang, F. Wang and L. M. Tolbert, "DQ Impedance Based Stability Analysis and Parameter Design of Three-Phase Inverter-Based AC Power Systems," in IEEE Trans. on Ind. Electron., vol. 64, no. 7, pp. 6017-6028, July 2017.

[11] B. Wen, D. Boroyevich, R. Burgos, P. Mattavelli and Z. Shen, "Inverse Nyquist Stability Criterion for Grid-Tied Inverters," IEEE Trans. on Power Electron., vol. 32, no. 2, pp. 1548-1556, Feb. 2017.

[12] B. Wen, D. Boroyevich, R. Burgos, P. Mattavelli and Z. Shen, "Small-Signal Stability Analysis of Three-Phase AC Systems in the Presence of Constant Power Loads Based on Measured d-q Frame Impedances," in IEEE Trans. on Power Electron., vol. 30, no. 10, pp. 5952-5963, Oct. 2015.

[13] B. Wen, D. Boroyevich, R. Burgos, P. Mattavelli and Z. Shen, "Analysis of D-Q Small-Signal Impedance of Grid-Tied Inverters," in IEEE Trans. on Power Electron., vol. 31, no. 1, pp. 675-687, Jan. 2016.
[14] G. O. Kalcon, G. P. Adam, O. Anaya-Lara, S. Lo and K. Uhlen, "Small-Signal Stability Analysis of Multi-Terminal VSC-Based DC Transmission Systems," in IEEE Trans. on Power Syst., vol. 27, no. 4, pp. 1818-1830, Nov. 2012.
[15] J. Beerten, S. D'Arco and J. A. Suul, "Identification and Small-Signal Analysis of Interaction Modes in VSC MTDC Systems," in IEEE Trans. on Power Del., vol. 31, no. 2, pp. 888-897, April 2016.
[16] K.N.B.M. Hasan, K. Rauma, A. Luna, J.I. Candela and P. Rodriguez, "Harmonic Compensation Analysis in Offshore Wind Power Plants Using Hybrid Filters," IEEE Trans. on Ind. Appl., vol.50, no.3, pp.2050,2060, May-June 2014
[17] L. Wang, X. Xie, Q. Jiang, H. Liu, Y. Li and H. Liu, "Investigation of SSR in Practical DFIG-Based Wind Farms Connected to a Series-Compensated Power System," in IEEE Trans. on Power Syst., vol. 30, no. 5, pp. 2772-2779, Sept. 2015.
[18] N. Prabhu and K.R. Padiyar "Investigation of Subsynchronous Resonance With VSC-Based HVDC Transmission Systems," IEEE Trans. on Power Del., vol.24, no.1, pp.433,440, Jan. 2009
[19] R.K. Varma, S. Auddy and Y. Semsedini, "Mitigation of Subsynchronous Resonance in a Series-Compensated Wind Farm Using FACTS Controllers," IEEE Trans. on Power Del., vol.23, no.3, pp.1645,1654, July 2008
[20] L. Fan and Z. Miao, "Mitigating SSR Using DFIG-Based Wind Generation," IEEE Trans. on Sust. Energy, vol.3, no.3, pp.349,358, July 2012
[21] G. Beccuti, G. Papafotiou and L. Harnefors, "Multivariable Optimal Control of HVDC Transmission Links With Network Parameter Estimation for Weak Grids," in IEEE Trans. on Control Syst. Technol., vol. 22, no. 2, pp. 676-689, March 2014.
[22] M. S. Chong, D. Nei, R. Postoyan and L. Kuhlmann, "Parameter and State Estimation of Nonlinear Systems Using a Multi-Observer Under the Supervisory Framework," in IEEE Trans. on Automat. Control, vol. 60, no. 9, pp. 2336-2349, Sept. 2015.
[23] L. Harnefors, M. Bongiorno and S. Lundberg, "Input-Admittance Calculation and Shaping for Controlled Voltage-Source Converters," in IEEE Trans. on Ind. Electron., vol. 54, no. 6, pp. 3323-3334, Dec. 2007.
[24] J. Huang, K. A. Corzine and M. Belkhayat, "Small-Signal Impedance Measurement of Power-Electronics-Based AC Power Systems Using Line-to-Line Current Injection," in IEEE Trans. on Power Electron., vol. 24, no. 2, pp. 445-455, Feb. 2009.
[25] G. Francis, R. Burgos, D. Boroyevich, F. Wang, and K Karimi, "An algorithm and implementation system for measuring impedance in the D-Q domain, "Energy Conversion Congress and Exposition (ECCE), 2011 IEEE , pp.3221 ,3228, 17-22 Sept. 2011.
[26] B. Wahlberg, "System identification using Kautz models," in IEEE Trans. on Automat. Control, vol. 39, no. 6, pp. 1276-1282, Jun 1994.
[27] P. Eykhoff, "System identification", Wiley, London, 1974
[28] David Chinarro, "System Engineering Applied to Fuenmayor Karst Aquifer (San Julin de Banzo, Huesca) and Collins Glacier (King George Island, Antarctica)", Springer International Publishing, Switzerland, 2014
[29] M. Amin, A. Rygg and M. Molinas, "Self-Synchronization of Wind Farm in an MMC-Based HVDC System: A Stability Investigation," in IEEE Trans. on Energy Convers., vol. 32, no. 2, pp. 458-470, June 2017.
[30] Q. C. Zhong and G. Weiss, "Synchronverters: Inverters That Mimic Synchronous Generators," in IEEE Trans. on Ind. Electron., vol. 58, no. 4, pp. 1259-1267, April 2011.

Mohammad Amin (M'11) was born in Chittagong, Bangladesh. He received the B.Sc. degree in electrical and electronic engineering from Chittagong University of Engineering and Technology, Chittagong, Bangladesh, the M.Sc. degree in electric power engineering from Chalmers University of Technology, Gothenburg, Sweden, and the Ph.D. in Engineering Cybernetics from Norwegian University of Science and Technology (NTNU), Trondheim, Norway in 2008, 2011 and 2017, respectively.

From 2008 to 2013, he was with the Department of Electrical and Electronic Engineering, International Islamic University Chittagong (IIUC) at Chittagong. In 2015, he was a Ph.D. Visiting Scholar with the Wind Power Research Center, Shanghai Jiao Tong University, Shanghai, China. Currently he is a senior research associate with the department of electrical and computer engineering at Illinois Institute of Technology in Chicago, USA. Dr. Amin's current research interest includes Power electronics application to power system, power converter control, HVDC, Smartgrid, Microgrid, Distributed Generation, and grid integration of wind/solar energy.

Marta Molinas (M'94) received the Diploma degree in electromechanical engineering from the National University of Asuncion, Asuncion, Paraguay, in 1992; the Master of Engineering degree from Ryukyu University, Japan, in 1997; and the Doctor of Engineering degree from the Tokyo Institute of Technology, Tokyo, Japan, in 2000.

She was a Guest Researcher with the University of Padova, Italy, during 1998. From 2004 to 2007, she was a Postdoctoral Researcher with the Norwegian University of Science and Technology (NTNU) and from 20082014 she has been professor at the Department of Electric Power Engineering at the same university. From 2008 to 2009, she was a Japan Society for the Promotion of Science (JSPS) Research Fellow with the Energy Technology Research Institute, National Institute of Advanced Industrial Science and Technology, Tsukuba, Japan. From 2013 to 2014, she was Visiting Professor at Columbia University and Invited Fellow by the Kingdom of Bhutan working with renewable energy microgrids for developing regions. She is currently Professor at the Department of Engineering Cybernetics, NTNU. Her research interests include stability of complex power electronics systems, harmonics, oscillatory phenomena, and nonstationary signals from the human and the machine.

Dr. Molinas has been an AdCom Member of the IEEE Power Electronics Society. She is Associate Editor and Reviewer for IEEE Transactions on Power Electronics, PELS Letters and the Journal of Emerging and Selected Topics in Power Electronics. She is also Editor of IEEE Transactions on Energy Conversion and Associate Editor of IEEE Transactions on Industrial Electronics. .